ACS Catalysis

Research Article

pubs.acs.org/acscatalysis

Design Principles of Heteroepitaxial Bimetallic Catalysts

Wei Guo,[†] Michail Stamatakis,[†,‡] and Dionisios G. Vlachos*[,†]

[†]Center for Catalytic Science and Technology, Department of Chemical and Biomolecular Engineering, University of Delaware, Newark, Delaware 19716, United States

[‡]Department of Chemical Engineering, University College London, Torrington Place, London WC1E 7JE, U.K.

Supporting Information

ABSTRACT: Heteroepitaxial bimetallic catalytic materials have been attracting considerable interest because of their unique properties and applications in energy, chemicals, and fuel sectors. Optimizing the activity of bimetallic catalysts requires the ability to understand and precisely manipulate the nanostructure (loading and dispersion of an admetal on a host metal). Ammonia decomposition catalyzed by Ni on Pt(111) [Ni/Pt(111)] is a prototype structure sensitive reaction for this purpose, in which both N−H bond breaking and N−N bond formation can be rate-limiting steps. Here, a first-principles kinetic Monte Carlo simulation framework reveals the bifunctional role of Ni clusters on Pt(111) in NH_3 decomposition: dehydrogenation on Ni terrace and N_2 desorption near Ni steps on Pt. We show that the dynamic interplay between surface nitrogen diffusion and association near the steps of Ni clusters and Pt terraces is responsible for the lower than expected nitrogen desorption temperature found in experiments. Our results illustrate the significance of metal loading and microstructure on macroscopic performance. A model is introduced with the aim of optimizing the bimetallic surface at nanoscale for improved reactivity. This simulation framework can be employed to understand and eventually tune bimetallic catalytic materials for arbitrarily complex chemistries.

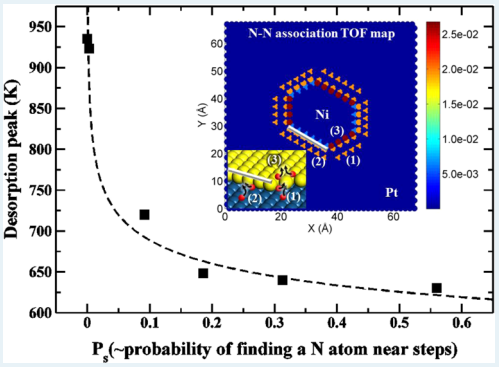

KEYWORDS: *bifunctional, bimetallic catalyst, nanostructure, Ni/Pt, ammonia decomposition, multiscale*

INTRODUCTION

Over the past decade, there has been growing interest in bimetallic catalysts because they can exhibit increased activity and/or reduced cost at comparable activity compared to single-metal catalysts. Among bimetallics, the surface [X−Y−Y (first layer−second layer−bulk)] or subsurface (Y−X−Y) bimetallics have attracted the most interest. In the former, a second metal resides atop a host metal [core−shell structure in the case of nanoparticles (see Figure 1)], whereas in the latter, a second metal is sandwiched between a core and a top layer of a host metal (core−shell−shell). Such structures possess unique properties that are not an interpolation between the parent metals of which they are made.[1−4] Such novel properties have been well demonstrated experimentally for several classes of reactions, including dehydrogenation (A−H bond scission, where A is a heteroatom, such as N, C, etc.),[5−7] reforming of various fuels (C−C bond scission),[8,9] water gas shift,[10] hydrogenation,[11] oxygen reduction reaction,[12] CO oxidation,[13] CO and CO_2 reduction,[14−18] electrocatalysis,[19,20] etc. Their unique properties have been attributed to the shift of the d-band center with respect to the Fermi level. As an example, it has been found that surface bimetallic Ni−Pt−Pt [a monolayer (ML) of Ni on top of Pt] is an excellent dehydrogenation catalyst in ammonia decomposition and reforming of biomass derivatives, producing hydrogen for fuel cells and upgrade of biomass, respectively.[5,21] Importantly, trends on single crystals often hold for supported catalysts in vapor or even aqueous phase chemistry.[21]

Density functional theory (DFT) and microkinetic modeling (detailed reaction mechanism) along with semiempirical methods have recently provided a computational platform for screening of bimetallics. These techniques combine informatics with a detailed chemical mechanism for identifying a suitable

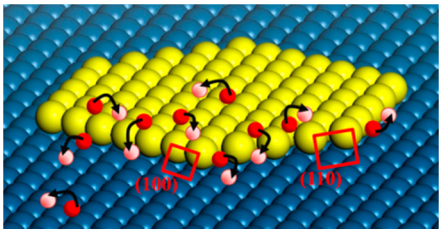

Figure 1. Side view of elementary steps of N* diffusion on a Ni cluster on Pt(111). There are two types of steps, (110) and (100). Yellow, blue, and red spheres represent Ni, Pt, and N atoms, respectively. The black arrows indicate N diffusion pathways, and pale red spheres represent the final positions of N atoms upon diffusion.

Received: July 5, 2013
Revised: August 25, 2013
Published: August 27, 2013

pair of metals and overall structures (surface or subsurface) for increased catalyst activity.[4,22,23] Several successes of model predictions have been demonstrated experimentally.[5,24] While this is an important milestone in our understanding and predicting novel materials for various chemistries, models have been rather limited because they have relied on ideal structures (full monolayer of a metal on a host). Real materials contain clusters of the second metal on a host (Figure 1), as shown using scanning tunneling microscopy (STM).[25] Experimental evidence indicates that incomplete ML of the second metal may be better;[26] however, the reasons remain elusive, and methods for selecting the amount of the surface metal do not currently exist. Tailoring materials for improved activity would require understanding the effect of nanostructure (coverage of second metal, cluster size, and shape effects).

In this paper, we introduce a general computational framework for exploring the effect of the nanostructure of the overlayer on a host metal on chemical activity. The framework relies on first-principles kinetic Monte Carlo (KMC) simulations that build upon a novel representation of nanostructure properties. We select the ammonia decomposition reaction as a test bed because it is known to be a structure sensitive reaction, and as such, it represents a fairly large class of reactions. Furthermore, certain bimetallic catalysts have already proven to be better than single-metal catalysts (e.g., Ni−Pt−Pt compared to Ru) for this reaction. Finally, temperature-programmed desorption (TPD) data provide a comprehensive database for assessing model predictions. We show unequivocally that common surface bimetallics can exhibit a bifunctional role whereby extended surfaces, such as terraces, perform most of the dehydrogenation and steps conduct desorption of N_2. Our results support for the first time the fact that control of nanostructure can markedly impact chemical activity, and we develop a simple yet powerful approach for optimizing nanostructures.

COMPUTATIONAL METHODS

N diffusion and association barriers were calculated using periodic spin-polarized DFT calculations via the Vienna *ab initio* simulation package (VASP, version 5.2.12).[27,28] The exchange correlation was described with the Revised Perdew−Burke−Ernzerhof parametrized generalized gradient approximation (GGA-RPBE) functional.[29] The electron−ion interactions were treated with pseudopotentials generated with the projector augmented wave (PAW) method,[30,31] and Kohn−Sham one-electron valence states were expanded in plane wave basis sets truncated at a cutoff energy of 350 eV. A higher cutoff, 396 eV, has been tested, and we found that the N_2 atomization energy and N binding energy on Pt(111) changes were less than 25 meV. The Fermi population of the Kohn−Sham state was calculated at an electronic temperature of k_BT = 0.1 eV, and all the potential energies were extrapolated to zero temperature. The surface Brillouin zone was sampled using a Monkhorst−Pack grid.[32] A 2 × 2 × 1 *k*-mesh was used, following convergence tests of nitrogen binding energies for similar systems.[5] For all types of surfaces, an interslab vacuum separation of 14 Å was used. The convergence criterion was set to 10^{-4} eV for the self-consistent electronic minimization and 0.1 eV/Å for the gradient in ionic relaxation. The latter was checked with 0.05 eV/Å, and the total energy change was less than 20 meV. The (111) surface was modeled using p(4 × 4) unit cells. All slabs consisted of four layers of metal substrate with the bottom two layers fixed to their bulk positions. To determine transition states (TSs), we have used the climbing image Nudged Elastic Band method (CI-NEB)[33] for nitrogen diffusion. The constrained minimization technique implemented in Atomic Simulation Environment (ASE)[34] was used for TS searching for surface nitrogen association. This method has been shown to be accurate for the calculation of reaction barriers in heterogeneous catalysis.[35] We took N_2 in the gas phase as the reference state. Zero-point energy (ZPE) corrections have been applied to all the energies.

At the molecular level, the reaction energetics were employed as inputs to a recently developed graph-theoretical KMC simulation framework.[36] The pre-exponentials were computed as ratios of quasi-partition functions of the transition state to those of the reactants. Lateral interactions were treated with a simple cluster expansion model, i.e., the lattice gas model with first nearest-neighbor pairwise additive interactions, $\Delta E(\theta) = \Delta E(\theta \sim 0) + \sum_{\text{pair}} n_{\text{pair}} \varepsilon_{\text{pair}}$, following recent work.[36,37] This approach takes into account the local adsorption configuration and lateral interactions and requires only a few calculations to parametrize the interactions. In most cases, the first nearest pair accounts for most of the coverage effects. The N−N pair interaction model was found to reproduce the coverage-dependent N binding energy on Ni/Pt(111).[38] In the TPD simulation, the time-dependent reaction rate constants were treated using the method reported in ref 39. KMC simulations were performed on three types of Pt(111) substrates: 6 × 6 size of p(4 × 4) (primitive hexagonal lattice), 2 × 2 size of c(7 × 12), and c(14 × 24) (centered rectangular lattice). Metal atoms are fixed during our KMC simulations, but the KMC framework is flexible to allow for metal atom mixing in future work. The surfaces had 576, 672, and 672 top layer Pt atoms, respectively. We considered 1728, 2016, and 2016 sites for the three Ni/Pt(111) surfaces, respectively. These sites entail fcc, hcp hollow, top, and step sites. In total, we considered 19 types of sites in our model: six, seven, four, and two types of fcc hollow, hcp hollow, top, and step sites, respectively. To avoid sampling of low-barrier diffusion processes only, we raised those lowest barriers, while keeping these processes well equilibrated and at least 2 orders of magnitude faster than the slower association processes. The initial nitrogen coverage was 0.3; the heating rate was 3 K/s, and 100 s was simulated in all the KMC runs. Because of the stochastic nature of KMC simulations, we have smoothed each TPD curve by averaging 20 KMC calculations employing different initial random seeds for the initialization of N adsorption sites.

RESULTS AND DISCUSSION

Ammonia decomposition proceeds via dehydrogenation ($NH_x^* + * \rightarrow NH_{x-1}^* + H^*$), followed by associations of N* and H* ($2N^* \rightarrow N_2 + 2^*$, and $2H^* \rightarrow H_2 + 2^*$), where * denotes a surface species or catalyst site. High-resolution electron energy loss spectroscopy (HREELS) results have shown that on Ru, the NH_x decomposition temperature is lower than 400 K and the NH_x coverage is 1 order of magnitude lower than that of N.[40] Thus, N−N bond formation from association of NH_x species is probably unimportant in ammonia decomposition under our conditions. The dissociation of NH_3 does not show strong structure dependence. For example, the NH dissociation barrier on Pt(211) is only 0.1 eV lower than on Pt(111), and neither (100) nor (211) surfaces facilitate the NH_2 dissociation with respect to Pt(111).[41] In addition, the largest barriers of N−H bond cleavage in NH_x show only a weak dependence on metal. For instance, on close-packed surfaces of Ni, Pd, Pt, Fe,

dx.doi.org/10.1021/cs4005166 | ACS Catal. 2013, 3, 2248−2255

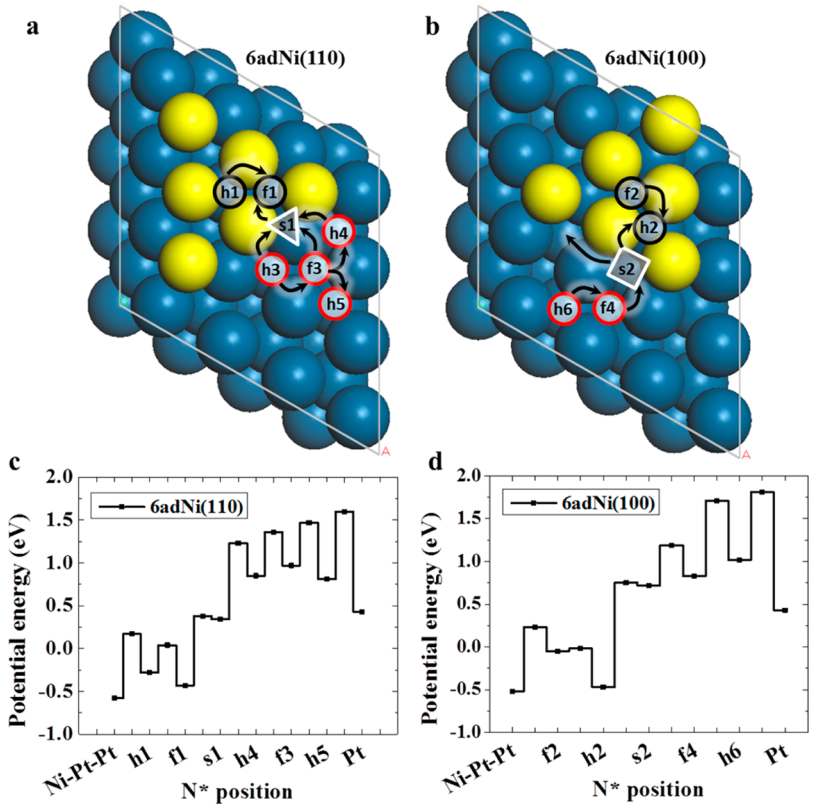

Figure 2. N* diffusion pathways and energy profiles. Diffusion close to a Ni cluster edge is modeled using two clusters of six Ni adatoms on Pt: 6adNi(110) and 6adNi(100), chosen to capture (110) and (100) steps, respectively. Hollow sites that are not close to steps are modeled as hollow sites of pure Pt or Ni−Pt−Pt surfaces. 6adNi(110) and 6adNi(100) have six (110) and (100) step sites as shown in panels a and b, respectively. The black circles represent hollow sites on Ni and red circles hollow sites on Pt. The white triangle and rectangle depict (110) and (100) step sites, respectively. The arrows in panels a and b indicate the diffusion from initial states to final states listed in Table S1 of the Supporting Information. (c and d) Energy profiles of the most preferred pathways of N diffusion on 6adNi(110) and 6adNi(100). "f","h", and "s" stand for fcc hollow, hcp hollow, and step sites, respectively. On larger clusters, N diffusions between the step and Ni or Pt terraces [h1 (or f2) ↔ Ni−Pt−Pt or h5 (or h6) ↔ Pt, respectively] are modeled from the energetics of a combination of 6adNi(110), 6adNi(100), pure Pt, and Ni−Pt−Pt. N_2 in the gas phase is the reference state.

Ru, Co, and Rh, the barriers are 1.1, 1.2, 1.4, 1.2, 1.2, 1.1, and 1.0 eV, respectively.[41−44] For Ni on Pt(111), the Ni terrace provides active sites for N−H bond breaking because of its stronger binding of NH_x species than on Pt. Besides dehydrogenation, N_2 desorption is another key step in ammonia decomposition. Association of surface N atoms with molecular nitrogen is believed to happen at the so-called B5-type step sites [at (100) steps]. The five metal atoms stabilize the association transition state at a pair of step and terrace sites.[45−48] The number of B5 sites is highly dependent on particle shape and size, resulting in structure sensitivity for N−N bond formation. For example, the N_2 association barrier on Pt(211) is 0.9 eV lower than on Pt(111).[49,50]

In vacuum, it is observed that adatoms tend to nucleate around defects or steps of a substrate. On (111) terraces of single crystals, the size of the (111) terrace can be tens of nanometers. Thus, Pt steps play only a minor role when depositing a Ni monolayer. The Ni−Pt−Pt structure is found to be stable at low temperatures, and monatomic steps have been observed at the edge of Ni terraces in STM experiments. Obviously, there are numerous cluster configurations one could consider. The structures considered here and in the Supporting Information are meant to illustrate the effect of clusters on the TPD spectra and activity of the catalyst compared to those of the idealized single monolayer considered in prior DFT and microkinetic (mean field) calculations. Upon being annealed to ∼600 K, Ni atoms diffuse into the Pt bulk and form a Pt−Ni−Pt structure.[25] A recent molecular dynamics (MD) simulation on the mixing between Ni and Pt atoms reveals that Ni can reside atop Pt as Ni clusters during the mixing.[51] In the presence of N atoms, such Ni clusters on Pt(111) are more energy favorable because N−Ni bonding is stronger than N−Pt bonding.[38] Figure 1 shows a single Ni cluster on Pt(111). N atoms may diffuse on a Ni terrace, on a Pt terrace, or along or across the steps. Previous calculations have shown that Ni atoms at the center of a large Ni cluster on Pt(111) are constrained to the underlying Pt lattice and strain release happens mostly at the cluster edge.[38] Thus, N energetics on the center of a large Ni cluster is similar to that on Ni−Pt−Pt, and N energetics at the edge of a large cluster can be approximated with that of N on small Ni clusters, where all the Ni atoms are edge atoms. To model all the processes shown in Figure 1, we calculate the binding energy, the transition states of N* association and diffusion on Pt, Ni−Pt−Pt, and two small Ni clusters on Pt consisting of different steps (Figure 2a,b). Because Ni atoms exhibit a higher d-band center than Pt atoms, the binding strength near steps is different from the corresponding sites of stepped pure metals. For instance, the step sites (s1 and s2 in Figure 2) bind N 0.77 and 0.96 eV weaker than Ni hollow sites near steps (f1 and h2), respectively.

dx.doi.org/10.1021/cs4005166 | ACS Catal. 2013, 3, 2248−2255

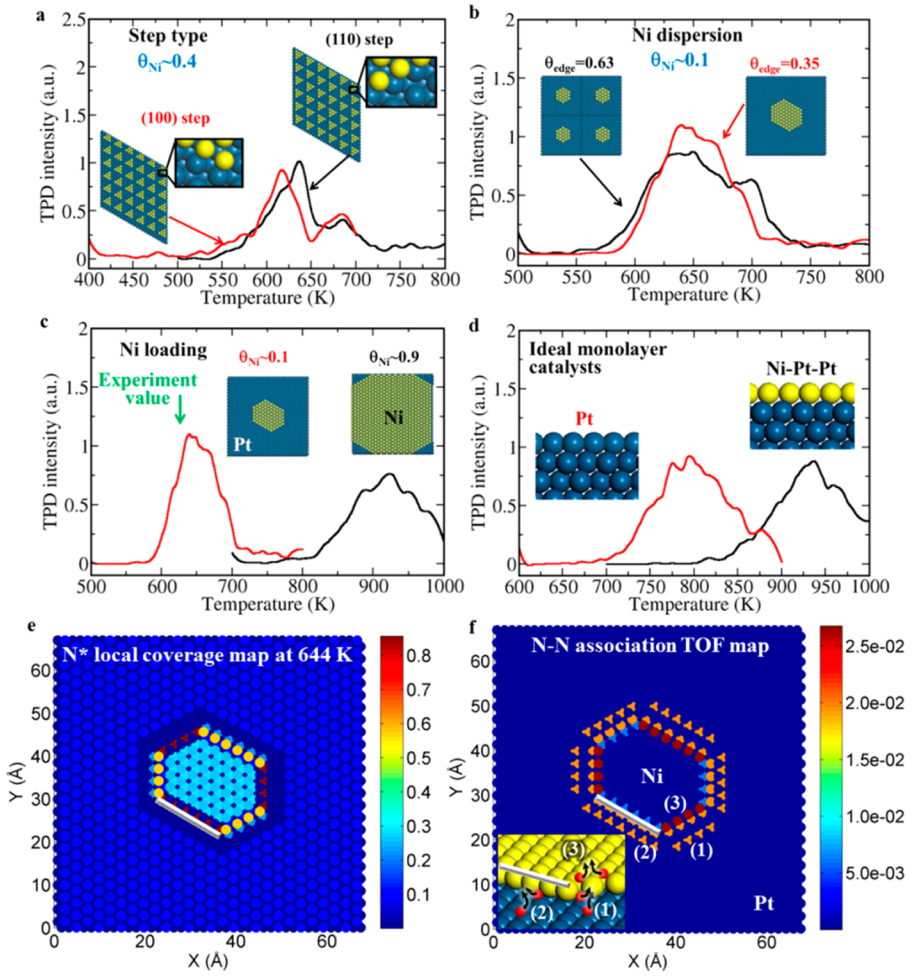

Figure 3. TPD simulations of N_2 desorption on different surfaces. (a) Effect of step type: 6adNi(110) with (110) steps only and 6adNi(100) with (100) steps only. (b) Effect of Ni dispersion: same θ_{Ni} but different θ_{edge}. (c) Effect of θ_{Ni}. The experimental value of the desorption peak temperature[5] is marked by the green arrow. (d) Terrace only: Pt and Ni−Pt−Pt. For the different Ni clusters on Pt(111) in panels a−c, top views are provided as insets. Instead, side views are provided for Pt and Ni−Pt−Pt surfaces in panel d. (e) Color maps of the N* local coverage at 644 K on the θ_{Ni} = 0.1 surface. The local coverage is normalized with respect to the number of sites for each site type. (f) Total N* association rate (events per second per site for each different site type) on the θ_{Ni} = 0.1 surface. The inset shows the corresponding structure of the map and three association channels. The white bars indicate one of the six edges of the hexagonal Ni cluster.

In contrast, on a stepped Ru(0001) surface, the corresponding s1 and s2 sites bind N only 0.09 and 0.29 eV weaker than the f1 and h2 sites, respectively.[52] On a Rh(211) step, the s2 site binds N only 0.34 eV weaker than the h2 site.[53]

N* Diffusion. The diffusion barriers are summarized in Table S1 of the Supporting Information and panels c and d of Figure 2. Similar to pure metals, transition states for diffusion involve bridge sites. Interestingly, we found a strong structural effect when correlating the potential energies of the transition state (TS) with those of the initial state (IS) (cf. the Supporting Information). This structural effect can be understood on the basis of the d-band theory. It is well-known that chemisorption energies correlate linearly with the d-band center for various adsorbates on transition metals.[54] For N adsorption and diffusion on Ru(0001), Hammer reported large differences in bonding among bridge, fcc, and hcp sites.[52] For instance, hcp sites bind atomic N 0.4 and 0.7 eV stronger than fcc and bridge sites, respectively (at the same d-band center of −2.0 eV). We find a similar trend for N binding. However, in our case (bulk Ni and Pt are fcc lattices), fcc hollow sites bind N slightly stronger than hcp sites (<0.2 eV) and ∼0.7 eV stronger than bridge sites. For diffusional hops between hollow sites, the TS has a N adatom on a bridge site. For terrace or terracelike structures, atoms in the IS and TS have the same d-band center. Thus, diffusion entails a barrier of ∼0.7 eV. For diffusion along the lower part of the steps, both Ni and Pt atoms near the step edges are involved. The upper Ni atoms of the step tend to decrease the TS potential energy because of the upward-shifted d-band center of these low-coordinate atoms. Thus, a lower diffusion barrier (∼0.4 eV) is found. For diffusion along or across Ni edge atoms, where only edge Ni atoms are involved, the diffusion barrier is even lower as a result of its early TS nature.

The effect of coverage on barriers has also been examined. The N binding energy decreases because of N−N repulsion, as do both the IS and TS potential energies. As a result, the diffusion barrier is only slightly affected. This coverage dependence is captured by the Brønsted−Evans−Polanyi (BEP) linear relation, in which the transition state potential energy can be interpolated from either the initial or the final state, depending on whether the TS is early or late along the reaction coordinate.[55,56]

The potential energy profiles of the most preferred N diffusion pathways are shown in panels c and d of Figure 2.

dx.doi.org/10.1021/cs4005166 | ACS Catal. 2013, 3, 2248−2255

Similar to stepped surfaces of pure metals, the barriers for attachment to and detachment from steps are asymmetric: attachment from the lower terrace to steps and detachment from steps to the lower terrace entail barriers larger than that on the upper terrace.[52] For Ni clusters on Pt(111), however, the difference is more pronounced than for pure metals. For example, the barrier for detachment from steps to the lower terrace (f1 to Pt) is more than 1 eV larger than from steps to the upper terrace (f1 to Ni−Pt−Pt). The energy profiles clearly show that N atoms tend to diffuse from Pt to Ni terraces by readily crossing the steps between them. Moreover, corner Ni atoms facilitate diffusion from Pt to step sites on 6adNi(110), following the f3 → h4 → s1 path. Given that Ni−Pt−Pt binds an N* 1 eV stronger than Pt (−0.58 vs 0.43 eV), it is expected that Ni clusters serve as a reservoir of N atoms. These findings differentiate bimetallic catalysts from stepped single metals.

N* Association. The structural sensitivity of N* association on single metals has been discussed extensively in lieu of ammonia synthesis.[55,57] We found a similar trend for Ni/Pt(111) bimetallic systems. On terraces, two N atoms reside at bridge or hollow sites at the TS. The association barriers are ∼2 eV, indicating that N atoms diffuse away from each other because of strong repulsion rather than recombination and desorption. At an interfacial pair of sites (a step site and a Pt terrace site, see s1-f3 or s2-f4 in panels a and b of Figure 2), the TS is stabilized by minimizing bond sharing between the two N atoms.[58] The TS energetics, structures, and energy diagram are shown in the Supporting Information. For 6adNi(110), the largest barriers for diffusion and association are 1.15 and 1.28 eV, respectively. For 6adNi(100), the corresponding barriers are 1.21 and 0.47 eV, respectively. As a result, desorption of N from either step site (s1 or s2) entails a lower apparent barrier than on a terrace, leading to fast desorption (see below). Because N* binds stronger on Ni than on Pt, association at interfacial sites has to be preceded by diffusion so that two N atoms encounter each other (see Figure S4 of the Supporting Information). Steps of Ni clusters on Pt(111) facilitate N_2 desorption in a manner different from that of pure metal steps, e.g., N association on Rh(211).[53] In particular, diffusion and spillover play an important role in bimetallics, because N atoms tend to reside on Ni rather than on Pt. On pure metals, on the other hand, the difference in binding energy between hollow sites below or above the step is smaller than that of steps of Ni/Pt(111).

KMC Simulations of TPD Spectra. Because N association is kinetically preferred at steps, we infer that the Ni coverage (θ_{Ni}) may affect the N_2 desorption temperature. N atoms occupy preferentially Ni hollow sites. At a high θ_{Ni}, spillover of N* from Ni to Pt terrace is difficult. Thus, Pt hollow sites near steps are rarely occupied, leading to a high desorption temperature. At a low θ_{Ni}, on the other hand, there are a limited number of interfacial sites, and thus, the desorption temperature may be as high as on pure Ni−Pt−Pt or Pt. To investigate the interplay of diffusion and association on the mechanism and, thus, to examine the effect of nanostructure on macroscopic behavior, we performed KMC simulations of nitrogen TPD spectra on Ni/Pt(111) with Ni cluster(s) of different sizes and shapes.

To quantitatively characterize the effect of microstructure (step types) for a fixed amount of Ni on Pt, we first simulate the TPD on 6adNi(110) and 6adNi(100) surfaces (Figure 3a). For each case, Ni atoms are edge atoms (Ni edge fraction, θ_{edge} = 1). Some N_2 desorption events are observed as early as 550−600 K in Figure 3a. The peaks between 600 and 650 K are attributed to the N* association at interfacial sites [channels (1) and (2) in Figure 3f]. However, the association barrier at interfacial sites of (100) steps is lower than that of (110) steps. Consequently, the peak for 6adNi(100) appears at a temperature ∼30 K lower than that of 6adNi(110). The occupation probability at steps sites is lower than that of Ni hollow sites; these association channels are unimportant as the coverage decreases (after 650 K). The peaks between 650 and 700 K in Figure 3a are attributed to the N* association at the Ni hollow sites near the step [channel (3) in Figure 3f].

To determine the effect of Ni dispersion, we fix θ_{Ni} and conduct simulations with different numbers of step sites (Figure 3b). For both cases, the peaks at 600 to 675 K correspond to N* association at interfacial sites [cf. channel (1) and channel (2) in Figure 3f]. The peaks above 675 K are mostly contributions from N* association at Ni fcc hollow sites near edge Ni atoms of (110) steps [cf. channel (3) in Figure 3f]. However, the black curve has a higher fraction of Ni edge atoms (θ_{edge}), indicating the higher probability of N_2 desorption near the steps and, thus, an early desorption peak.

Next we examine the effect of Ni coverage θ_{Ni} by increasing the size of the Ni cluster while fixing the step density. Figure 3c shows that when θ_{Ni} is sufficiently large (near 1 ML) to hold most surface N atoms, N_2 desorption predominantly happens from the Ni terrace (black curve in Figure 3c). The desorption peak ($\theta_{Ni} \sim 0.9$) appears at ∼925 K, 300 K higher than that from steps (red curve in Figure 3c, same as the red curve in Figure 3b). This high desorption temperature results from the fact that nitrogen atoms are mostly diffusing on the Ni terrace rather than associating below 850 K. The coverage of Ni drastically affects the N_2 desorption temperature.

The results at the 0 or 1 ML limit of θ_{Ni} (for Pt and Ni−Pt−Pt) are shown in Figure 3d. The N_2 association barriers on Pt and Ni−Pt−Pt surfaces are 1.96 and 2.29 eV, respectively, and the desorption peaks appear near 770 and 940 K, respectively. In NH_3 decomposition, Hansgen et al. reported experimentally a N_2 desorption temperature on Ni−Pt−Pt of 630 K and no chemistry on Pt(111).[5] The former is in remarkable quantitative agreement with our TPD calculations in panels a and b of Figure 3. For Pt(111), the absence of the N_2 peak is due to the weak NH_3 adsorption energy, resulting in a lack of decomposition. Our TPD simulations indicate that the low experimentally observed N_2 desorption peak of 630 K on Ni−Pt−Pt is attributed to Ni clusters on Pt(111); even if a full ML of Ni is deposited, Ni adatoms start diffusing into Pt at ∼600 K, creating an incomplete Ni ML.[59] We propose that such partial ML structures form either in the synthesis or by diffusion of the surface metal toward the bulk (given that the time scale for mixing[51] is comparable to that of a TPD experiment) that result in the very high activity of the bimetallic catalyst seen experimentally.

To visualize the active sites for N* associative desorption, we take the $\theta_{Ni} \sim 0.1$ and $\theta_{edge} = 0.35$ structure as an example. Spatial maps of N* local coverage and association rate are shown in panels e and f of Figure 3. Figure 3e demonstrates that, close to the desorption peak temperature, Ni edge sites exhibit the highest coverage: the brown sites [Ni hollow sites near the (100) step; cf. site h2 in Figure 2b] followed by the yellow sites [Ni hollow sites near the (110) step site; cf. site f1 in Figure 2a]. The coverage on the Ni terrace is lower than that of Ni edge sites but higher than on the Pt terrace. Furthermore, Figure 3f clearly shows that most association events happen at

dx.doi.org/10.1021/cs4005166 | ACS Catal. 2013, 3, 2248−2255

the interfacial pair of sites [channels (1) and (2)] and Ni hollow sites near the (110) step [channel (3)].

It is important to discuss the stability of Ni clusters on Pt(111). It has been reported experimentally that Ni may exchange with Pt atoms (Pt segregates to the surface layer) when 0.2 ML of Ni is deposited on Pt at 300 K in vacuum.[60] Higher Ni coverages raise the exchange barrier because of the Ni−Ni interaction, as seen in the Ni/Cu system.[15] We studied the effect of such Ni−Pt exchange in the center of the Ni cluster and found that the simulated TPD peak shifts only slightly to higher temperatures (Figure S5 of the Supporting Information). Although the Pt−Ni−Pt structure is thermodynamically favorable in vacuum, DFT calculations have shown that when the N coverage is larger than ∼0.3, the Ni−Pt−Pt structure becomes favorable.[61] In our simulations, we start with N coverage of 0.3 ML found in experiments (dose of ammonia of $\sim 10^{-8}$ Torr for 300 s). Thus, the Pt−Ni intermixing starting temperature must be higher than in vacuum. Such an effect has been seen in CO adsorption in the Ni/Cu system, where CO−Ni binding stabilizes Ni atoms in the surface layers,[18] and the surface coverage of Ni depends strongly on the CO partial pressure.[17] High temperatures make it challenging to maintain the active sites of catalysts. However, the nitrogen desorption peak temperature is ∼640 K, which is only 40 K higher than the Pt segregation temperature under clean catalyst conditions. Given that the N coverage is ∼0.3, we believe that partial ML structures form under practical catalytic UHV conditions, and this is the reason why Ni on Pt is so active. Thus, the model system (Ni cluster on Pt) in this work should be a reasonable representation of catalytic activity.

It has also been reported that surface hydrogen atoms may lower the self-diffusion barriers of metal adatoms through H−metal complexes ("skyhook" effect). For example, the Pt self-diffusion on Pt(110)−(1 × 2) is enhanced by formation of the Pt−H complex[62] by a reduction in the diffusion barrier of ∼0.1 eV. A similar H skyhook effect is also observed on Ni(100).[63] In our system, the H−H recombination barrier is so low that in TPD experiments, the desorption temperature of H_2 is low [e.g., ∼350 K on Pt(111)].[64] As a result, there is no H left when N desorption occurs. Given the high Ni diffusion barrier on Pt (∼1.7 eV[51]), hydrogen plays a minor role in Ni−Pt intermixing.

Next we focus on the relationship between Ni cluster microstructure (size and shape) and N_2 desorption temperature and provide a method for optimizing the nanostructure for better activity. The desorption turnover frequency (TOF) can be evaluated as

$$\mathrm{TOF} \propto \sum_{i=\mathrm{pathway}} p_i[\mathrm{N}^*_{(1)}-\mathrm{N}^*_{(2)}]\frac{k_B T}{h}\exp[-E_{a,i}/(k_B T)] \quad (1)$$

and entails the probability of finding an N*−N* pair p_i [$N^*_{(1)}$−$N^*_{(2)}$] multiplied by the rate constant. This is a generalized Arrhenius equation regardless of island shape and size. To describe the effect of microstructure, a structural parameter P_s is defined, which is the fraction of edge Ni atoms (θ_{edge}) and the coverage of exposed Pt, θ_{Pt} ($\theta_{Pt} + \theta_{Ni} = 1$):

$$P_s = \theta_{edge}(1 - \theta_{Ni}) \quad (2)$$

P_s measures the probability of finding a single N* near steps (see the Supporting Information). For different Ni coverages, the fraction of Ni edge atoms depends on the shape and number of clusters.

Figure 4 indicates that clusters with higher θ_{edge} values tend to have lower nitrogen desorption temperatures; interfacial sites

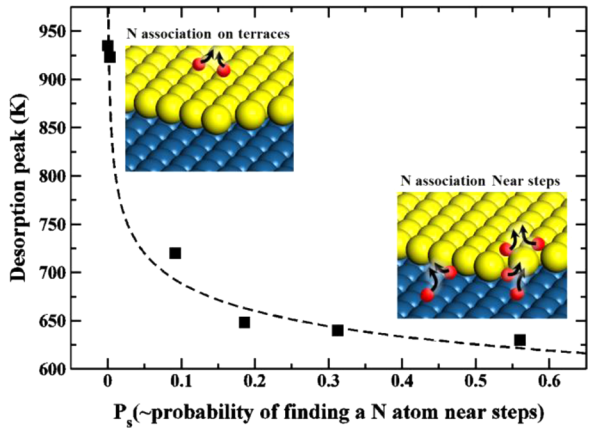

Figure 4. Relation between the structural parameter P_s and simulated N_2 desorption peak temperature for different Ni clusters on Pt(111). The dotted line is the fitted curve from Redhead's analysis of TPD (cf. the Supporting Information for details).

facilitate nitrogen association, and increasing their fraction is desirable. A high θ_{Ni} leads to low N coverage on Pt, and accordingly, interfacial sites are rarely occupied. As a result, without association channels near steps, N_2 desorption happens only from Ni terraces at high temperatures. To attain large θ_{edge}, Ni clusters should be small. The fitted curve in Figure 4 allows optimization of Ni cluster shape and coverage from a handful of KMC simulations (Figure S6 of the Supporting Information). Our simulations indicate that small clusters at low Ni coverage (<0.5) are preferred for desorption, but a sufficient number of Ni atoms on Pt is needed to adsorb and decompose NH_3. In our calculations in the Supporting Information, we show that the cluster shape plays a secondary role. This is because the desorption temperature is less sensitive to the cluster shape as compared to Ni coverage. For $\theta_{Ni} \sim 0.5$, we find narrow stripes to be optimal among triangles, hexagons, and stripes.

In experiments, Ni loading has been reported to play a role. For example, Yu et al. recently reported that 0.5 ML of Ni on tungsten carbide (WC, which possesses some Pt-like properties) shows enhanced syngas production of acetic acid decomposition over 1 ML and a thick Ni film.[26] Our results are qualitatively consistent with this experimental observation and provide a platform for optimizing the nanostructure of bimetallic catalysts.

CONCLUSIONS

By employing multiscale modeling, we investigated the TPD spectra of desorption of nitrogen from Ni clusters of different sizes and shapes on Pt(111). We showed that nitrogen association barriers near steps are lower than those on terraces, and thus, the steps of Ni clusters on Pt(111) are essential for N_2 desorption at temperatures of <700 K found experimentally. Desorption from steps involves a pair of step and Pt terrace sites or a pair of near-edge Ni hollow sites and has to be preceded by diffusion. Diffusion barriers are structure sensitive. In particular, N atoms diffuse from Pt terraces to Ni clusters by readily crossing the steps. The reverse diffusion (spillover from Ni to Pt) is difficult yet important for N_2 desorption, because N* binds stronger on Ni. Diffusion parallel to the step (on both

dx.doi.org/10.1021/cs4005166 | ACS Catal. 2013, 3, 2248−2255

upper Ni and lower Pt atoms) also entails lower barriers than on Pt or Ni terraces. The diffusion time from Ni clusters to edges leads to Ni cluster size-dependent reactivity. The asymmetric diffusion and adsorbate distribution on the surface, caused by the difference in the d-band centers of the metals, differs from N_2 desorption at steps of pure metals. Overall, our multiscale simulation identifies the active sites and the bifunctional role of Ni/Pt(111) in ammonia decomposition, whereby NH_3 decomposes on Ni clusters because of its stronger adsorption. Nitrogen is mainly bound on Ni, and desorption occurs primarily from cluster steps via spillover of N* from Ni to Pt. Our results indicate for the first time that there should be an optimal coverage and microstructure of the second material (Ni) on the host (Pt) in ammonia decomposition. Our simulation framework can be employed to understand and eventually tune bimetallic catalytic materials for arbitrarily complex chemistries.

■ ASSOCIATED CONTENT

Supporting Information

Effect of structure in N* diffusion, transition state energetics, structures, and energy diagram, effect of Ni−Pt exchange in the center of Ni cluster, and structural parameters of Ni clusters. This material is available free of charge via the Internet at http://pubs.acs.org.

■ AUTHOR INFORMATION

Corresponding Author

*E-mail: vlachos@udel.edu.

Notes

The authors declare no competing financial interests.

■ ACKNOWLEDGMENTS

The research was supported, in part, by the National Science Foundation (Grant CMMI-0835673). The DFT calculations were conducted at the Center for Functional Nanomaterials, Brookhaven National Laboratory (Upton, NY) (supported by the U.S. Department of Energy, Office of Basic Energy Sciences, under Contract DE-AC02-98CH10886), and the TeraGrid provided by the Texas Advanced Computing Center (TACC) of The University of Texas at Austin (Austin, TX).

■ REFERENCES

(1) Kitchin, J. R.; Norskov, J. K.; Barteau, M. A.; Chen, J. G. *J. Chem. Phys.* **2004**, *120* (21), 10240−10246.
(2) Chen, J. G.; Menning, C. A.; Zellner, M. B. *Surf. Sci. Rep.* **2008**, *63* (5), 201−254.
(3) Yu, W.; Porosoff, M. D.; Chen, J. G. *Chem. Rev.* **2012**, *112* (11), 5780−5817.
(4) Greeley, J.; Mavrikakis, M. *Nat. Mater.* **2004**, *3* (11), 810−815.
(5) Hansgen, D. A.; Vlachos, D. G.; Chen, J. G. G. *Nat. Chem.* **2010**, *2* (6), 484−489.
(6) Siri, G. J.; Ramallo-Lopez, J. M.; Casella, M. L.; Fierro, J. L. G.; Requejo, F. G.; Ferretti, O. A. *Appl. Catal., A* **2005**, *278* (2), 239−249.
(7) Salciccioli, M.; Yu, W. T.; Barteau, M. A.; Chen, J. G. G.; Vlachos, D. G. *J. Am. Chem. Soc.* **2011**, *133* (20), 7996−8004.
(8) Skoplyak, O.; Menning, C. A.; Barteau, M. A.; Chen, J. G. G. *J. Chem. Phys.* **2007**, *127*, 11.
(9) Ni, M.; Leung, D. Y. C.; Leung, M. K. H. *Int. J. Hydrogen Energy* **2007**, *32* (15), 3238−3247.
(10) Knudsen, J.; Nilekar, A. U.; Vang, R. T.; Schnadt, J.; Kunkes, E. L.; Dumesic, J. A.; Mavrikakis, M.; Besenbacher, F. *J. Am. Chem. Soc.* **2007**, *129* (20), 6485−6490.
(11) Murillo, L. E.; Goda, A. M.; Chen, J. G. *J. Am. Chem. Soc.* **2007**, *129* (22), 7101−7105.
(12) Stephens, I. E. L.; Bondarenko, A. S.; Perez-Alonso, F. J.; Calle-Vallejo, F.; Bech, L.; Johansson, T. P.; Jepsen, A. K.; Frydendal, R.; Knudsen, B. P.; Rossmeisl, J.; Chorkendorff, I. *J. Am. Chem. Soc.* **2011**, *133* (14), 5485−5491.
(13) Mu, R. T.; Fu, Q. A.; Xu, H.; Zhang, H. I.; Huang, Y. Y.; Jiang, Z.; Zhang, S. O.; Tan, D. L.; Bao, X. H. *J. Am. Chem. Soc.* **2011**, *133* (6), 1978−1986.
(14) Vesselli, E.; Monachino, E.; Rizzi, M.; Furlan, S.; Duan, X.; Dri, C.; Peronio, A.; Africh, C.; Lacovig, P.; Baldereschi, A.; Comelli, G.; Peressi, M. *ACS Catal.* **2013**, *3* (7), 1555−1559.
(15) Rizzi, M.; Furlan, S.; Peressi, M.; Baldereschi, A.; Dri, C.; Peronio, A.; Africh, C.; Lacovig, P.; Vesselli, E.; Comelli, G. *J. Am. Chem. Soc.* **2012**, *134* (40), 16827−16833.
(16) Nerlov, J.; Chorkendorff, I. *J. Catal.* **1999**, *181* (2), 271−279.
(17) Nerlov, J.; Chorkendorff, I. *Catal. Lett.* **1998**, *54* (4), 171−176.
(18) Nerlov, J.; Sckerl, S.; Wambach, J.; Chorkendorff, I. *Appl. Catal., A* **2000**, *191* (1−2), 97−109.
(19) Kowal, A.; Li, M.; Shao, M.; Sasaki, K.; Vukmirovic, M. B.; Zhang, J.; Marinkovic, N. S.; Liu, P.; Frenkel, A. I.; Adzic, R. R. *Nat. Mater.* **2009**, *8* (4), 325−330.
(20) Strasser, P.; Koh, S.; Anniyev, T.; Greeley, J.; More, K.; Yu, C. F.; Liu, Z. C.; Kaya, S.; Nordlund, D.; Ogasawara, H.; Toney, M. F.; Nilsson, A. *Nat. Chem.* **2010**, *2* (6), 454−460.
(21) Tupy, S.; Karim, A.; Bagia, C.; Deng, W.; Huang, Y.; Vlachos, D.; Chen, J. G. *ACS Catal.* **2012**, *2* (11), 2290−2296.
(22) Jacobsen, C. J. H.; Dahl, S.; Clausen, B. S.; Bahn, S.; Logadottir, A.; Norskov, J. K. *J. Am. Chem. Soc.* **2001**, *123* (34), 8404−8405.
(23) Maestri, M.; Reuter, K. *Angew. Chem., Int. Ed.* **2011**, *50* (5), 1194−1197.
(24) Studt, F.; Abild-Pedersen, F.; Wu, Q.; Jensen, A. D.; Temel, B.; Grunwaldt, J.-D.; Nørskov, J. K. *J. Catal.* **2012**, *293*, 51−60.
(25) Kitchin, J. R.; Khan, N. A.; Barteau, M. A.; Chen, J. G.; Yakshinksiy, B.; Madey, T. E. *Surf. Sci.* **2003**, *544* (2−3), 295−308.
(26) Yu, W. T.; Mellinger, Z. J.; Barteau, M. A.; Chen, J. G. G. *J. Phys. Chem. C* **2012**, *116* (9), 5720−5729.
(27) Kresse, G.; Furthmüller, J. *Phys. Rev. B* **1996**, *54* (16), 11169−11186.
(28) Kresse, G.; Furthmüller, J. *Comput. Mater. Sci.* **1996**, *6* (1), 15−50.
(29) Hammer, B.; Hansen, L. B.; Nørskov, J. K. *Phys. Rev. B* **1999**, *59* (11), 7413−7421.
(30) Blöchl, P. E. *Phys. Rev. B* **1994**, *50* (24), 17953−17979.
(31) Kresse, G.; Joubert, D. *Phys. Rev. B* **1999**, *59* (3), 1758−1775.
(32) Monkhorst, H. J.; Pack, J. D. *Phys. Rev. B* **1976**, *13* (12), 5188−5192.
(33) Henkelman, G.; Uberuaga, B. P.; Jonsson, H. *J. Chem. Phys.* **2000**, *113* (22), 9901−9904.
(34) Bahn, S. R.; Jacobsen, K. W. *Comput. Sci. Eng.* **2002**, *4* (3), 56−66.
(35) Liu, Z. P.; Hu, P. *J. Am. Chem. Soc.* **2003**, *125* (7), 1958−1967.
(36) Stamatakis, M.; Vlachos, D. G. *J. Chem. Phys.* **2011**, *134* (21), 214115.
(37) Stamatakis, M.; Chen, Y.; Vlachos, D. G. *J. Phys. Chem. C* **2011**, *115* (50), 24750−24762.
(38) Guo, W.; Vlachos, D. G. *J. Chem. Phys.* **2013**, *138* (17), 174702.
(39) Jansen, A. P. J. *Comput. Phys. Commun.* **1995**, *86* (1−2), 1−12.
(40) Dietrich, H.; Jacobi, K.; Ertl, G. *J. Chem. Phys.* **1997**, *106* (22), 9313−9319.
(41) Offermans, W. K.; Jansen, A. P. J.; van Santen, R. A.; Novell-Leruth, G.; Ricart, J. M.; Pérez-Ramírez, J. *J. Phys. Chem. C* **2007**, *111* (47), 17551−17557.
(42) Duan, X. Z.; Ji, J.; Qian, G.; Fan, C.; Zhu, Y.; Zhou, X. G.; Chen, D.; Yuan, W. K. *J. Mol. Catal. A: Chem.* **2012**, *357*, 81−86.
(43) Logadottir, A.; Norskov, J. K. *J. Catal.* **2003**, *220* (2), 273−279.
(44) Novell-Leruth, G.; Valcarcel, A.; Perez-Ramirez, J.; Ricart, J. M. *J. Phys. Chem. C* **2007**, *111* (2), 860−868.

(45) Jacobsen, C. J. H.; Dahl, S.; Hansen, P. L.; Tornqvist, E.; Jensen, L.; Topsoe, H.; Prip, D. V.; Moenshaug, P. B.; Chorkendorff, I. *J. Mol. Catal. A: Chem.* **2000**, *163* (1−2), 19−26.
(46) Karim, A. M.; Prasad, V.; Mpourmpakis, G.; Lonergan, W. W.; Frenkel, A. I.; Chen, J. G.; Vlachos, D. G. *J. Am. Chem. Soc.* **2009**, *131* (34), 12230−12239.
(47) Garcia-Garcia, F. R.; Guerrero-Ruiz, A.; Rodriguez-Ramos, I. *Top. Catal.* **2009**, *52* (6−7), 758−764.
(48) Schuth, F.; Palkovits, R.; Schlogl, R.; Su, D. S. *Energy Environ. Sci.* **2012**, *5* (4), 6278−6289.
(49) Bligaard, T.; Nørskov, J. K.; Dahl, S.; Matthiesen, J.; Christensen, C. H.; Sehested, J. *J. Catal.* **2004**, *224* (1), 206−217.
(50) Munter, T. R.; Bligaard, T.; Christensen, C. H.; Norskov, J. K. *Phys. Chem. Chem. Phys.* **2008**, *10* (34), 5202−5206.
(51) Wang, H. Y.; Stamatakis, M.; Hansgen, D. A.; Caratzoulas, S.; Vlachos, D. G. *J. Chem. Phys.* **2010**, *133* (22), 224503.
(52) Hammer, B. *Surf. Sci.* **2000**, *459* (3), 323−348.
(53) Inderwildi, O. R.; Jenkins, S. J.; King, D. A. *J. Am. Chem. Soc.* **2008**, *130* (7), 2213−2220.
(54) Bligaard, T.; Nørskov, J. K. Heterogeneous catalysis. In *Chemical Bonding at Surfaces and Interfaces*; Elsevier: Amsterdam, 2008; Chapter 4, pp 255−321.
(55) van Santen, R. A.; Neurock, M.; Shetty, S. G. *Chem. Rev.* **2010**, *110* (4), 2005−2048.
(56) Michaelides, A.; Liu, Z. P.; Zhang, C. J.; Alavi, A.; King, D. A.; Hu, P. *J. Am. Chem. Soc.* **2003**, *125* (13), 3704−3705.
(57) Norskov, J. K.; Bligaard, T.; Logadottir, A.; Bahn, S.; Hansen, L. B.; Bollinger, M.; Bengaard, H.; Hammer, B.; Sljivancanin, Z.; Mavrikakis, M.; Xu, Y.; Dahl, S.; Jacobsen, C. J. H. *J. Catal.* **2002**, *209* (2), 275−278.
(58) Ge, Q.; Neurock, M. *J. Am. Chem. Soc.* **2004**, *126* (5), 1551−1559.
(59) Menning, C. A.; Chen, J. G. *J. Chem. Phys.* **2008**, *128*, 16.
(60) Gambardella, P.; Kern, K. *Surf. Sci.* **2001**, *475* (1−3), L229−L234.
(61) Hansgen, D. A.; Vlachos, D. G.; Chen, J. G. G. *Surf. Sci.* **2011**, *605* (23−24), 2055−2060.
(62) Horch, S.; Lorensen, H. T.; Helveg, S.; Laegsgaard, E.; Stensgaard, I.; Jacobsen, K. W.; Norskov, J. K.; Besenbacher, F. *Nature* **1999**, *398* (6723), 134−136.
(63) Haug, K.; Zhang, Z.; John, D.; Walters, C. F.; Zehner, D. M.; Plummer, W. E. *Phys. Rev. B* **1997**, *55* (16), R10233−R10236.
(64) Poelsema, B.; Lenz, K.; Comsa, G. *J. Phys.: Condes. Matter* **2010**, *22* (30), 304006.